Published in final edited form as:
NMR Biomed. 2012 November ; 25(11): 1280–1285. doi:10.1002/nbm.2799.

Inhibition of the sodium–calcium exchanger via SEA0400 altered manganese-induced T_1 changes in isolated perfused rat hearts

Ya Chen[a,b], **Kevin Payne**[a], **Vindya S. Perara**[c], **Songping Huang**[c], **Akemichi Baba**[d], **Toshio Matsuda**[d], and **Xin Yu**[a,b,e,f,*]

[a]Department of Biomedical Engineering, Case Western Reserve University, Cleveland, OH, USA

[b]Case Center for Imaging Research, Case Western Reserve University, Cleveland, OH, USA

[c]Department of Chemistry, Kent State University, Kent, OH, USA

[d]Graduate School of Pharmaceutical Sciences, Osaka University, Osaka, Japan

[e]Department of Radiology, Case Western Reserve University, Cleveland, OH, USA

[f]Department of Physiology and Biophysics, Case Western Reserve University, Cleveland, OH, USA

Abstract

Manganese (Mn^{2+})-enhanced MRI (MEMRI) provides the potential for the *in vivo* evaluation of calcium (Ca^{2+}) uptake in the heart. Recent studies have also suggested the role of the sodium–calcium (Na^{+}–Ca^{2+}) exchanger (NCX) in Mn^{2+} retention, which may have an impact on MEMRI signals. In this study, we investigated whether MEMRI with fast T_1 mapping allowed the sensitive detection of changes in NCX activity. We quantified the dynamics of the Mn^{2+}-induced T_1 changes in isolated perfused rat hearts in response to SEA0400, an NCX inhibitor. The experimental protocol comprised 30 min of Mn^{2+} perfusion (wash-in), followed by a 30-min wash-out period. There were three experimental groups: 1, NCX inhibition by 1 μM SEA0400 during Mn^{2+} wash-in only (SEAin, $n = 6$); 2, NCX inhibition by 1 μM SEA0400 during Mn^{2+} wash-out only (SEAout, $n = 6$); 3, no NCX inhibition during both wash-in and wash-out to serve as the control group (CNTL, $n = 5$). Rapid T_1 mapping at a temporal resolution of 3 min was performed throughout the perfusion protocol using a triggered saturation–recovery Look–Locker sequence. Our results showed that NCX inhibition during Mn^{2+} wash-in caused a significant increase in relaxation rate (R_1) at the end of Mn^{2+} perfusion. During the wash-out period, NCX inhibition led to less reduction in R_1. Further analysis of Mn^{2+} content in myocardium with flame atomic absorption spectroscopy was consistent with the MRI findings. These results suggest that Mn^{2+} accumulation and retention in rat hearts are, in part, dependent on NCX activity. Hence, MEMRI may provide an imaging method that is also sensitive to changes in NCX activity.

Keywords

manganese-enhanced MRI; calcium uptake; sodium–calcium exchanger; T_1 mapping

INTRODUCTION

Cardiac excitation–contraction (EC) coupling, the process that converts an electrical stimulus to muscle contraction, is fundamental to ventricular function. Calcium (Ca^{2+}), the

*Correspondence to: X. Yu, Wickenden 430, 10900 Euclid Avenue, Cleveland, OH 44106, USA. xin.yu@case.edu.

ubiquitous second messenger that directly activates myofilaments, is of key importance in EC coupling (1). During a cardiac action potential, Ca^{2+} influx, mostly via the voltage-sensitive L-type Ca^{2+} channels, triggers Ca^{2+} release from the sarcoplasmic reticulum (SR), leading to a transient increase in cytosolic Ca^{2+} concentration during systole. During diastole, Ca^{2+} is removed from the cytosol, mostly through the Ca^{2+}-ATPase located in the SR and the sarcolemmal sodium–calcium (Na^{+}–Ca^{2+}) exchanger (NCX) (2,3). Myocardial contractility is dependent on the total Ca^{2+} concentration which must be supplied to and removed from the cytosol during each heart beat. Abnormal Ca^{2+} cycling has been implicated in contractile dysfunction (4).

The current investigation of Ca^{2+} cycling largely relies on the characterization of isolated cells or *ex vivo* hearts using fluorescent dyes or electrophysiological methods (5–7). Recently, manganese (Mn^{2+})-enhanced MRI (MEMRI) has been proposed for the *in vivo* evaluation of Ca^{2+} cycling in the heart (8). Mn^{2+} is a potent T_1-shortening agent (9). Unlike a gadolinium (Gd)-based contrast agent that is confined to the extracellular space, Mn^{2+} enters the cell through L-type Ca^{2+} channels (10,11) and perhaps NCX (12). Thus, it offers the unique opportunity for the *in vivo* delineation of an important cellular process that initiates EC coupling. Several studies have shown that the MEMRI signal reflects changes in Ca^{2+} uptake in the myocardium *in vivo* (13,14). More recently, Waghorn *et al.* (15,16) have also observed T_1 changes associated with Mn^{2+} efflux via the NCX 1 h after the withdrawal of Mn^{2+}. Their observation suggests that MEMRI may also be used for the evaluation of NCX activity, another important determinant of Ca^{2+} cycling. However, significantly higher temporal resolution and sensitivity are required to evaluate Mn^{2+} transport via NCX without prolonged imaging times.

In the current study, we evaluated the potential of MEMRI for the sensitive delineation of NCX activity via fast T_1 mapping. We hypothesized that Mn^{2+} accumulation and retention in cardiomyocytes were dependent on Mn^{2+} efflux via the NCX, which can be calculated from Mn^{2+}-induced T_1 changes. Using a fast T_1 mapping method, we quantified the dynamics of Mn^{2+}-induced T_1 changes in isolated perfused rat hearts in response to SEA0400, an NCX inhibitor (17), during Mn^{2+} perfusion (wash-in) and wash-out. Myocardial Mn^{2+} content was also measured by flame atomic absorption spectrophotometry to validate the findings by MRI. In addition, the cardiotoxicity of Mn^{2+} was evaluated in isolated cardiac myocytes exposed to 50–500 μM Mn^{2+}. These results will contribute to our understanding of the cellular processes that may have an impact on MEMRI measurements.

MATERIALS AND METHODS

Heart perfusion protocol

Male Sprague–Dawley rats (8–10 weeks) were heparinized (1000 units/kg, intraperitoneally) and anesthetized by sodium pentobarbital (85 mg/kg, intraperitoneally). The heart was excised, cannulated and perfused with Krebs–Henseleit (KH) buffer containing (in mM): NaCl, 118.5; KCl, 4.7; $MgSO_4$, 1.2; KH_2PO_4, 1.2; $CaCl_2$, 1.5; glucose, 11.1; $NaHCO_3$, 25. The perfusate was maintained at 37 °C and equilibrated with 95% O_2–5% CO_2. The perfusion pressure was maintained at a constant level (100 cmH_2O). A water-filled latex balloon was inserted into the left ventricle and connected to a pressure transducer to record the left ventricular end-diastolic pressure (LVEDP), left ventricular systolic pressure (LVSP) and heart rate (HR). The left ventricular developed pressure (LVDP) was calculated as the difference between LVSP and LVEDP. The rate–pressure product (RPP), i.e. the product of LVDP and HR, was calculated as an index of the workload.

Hearts were paced at 360 beats/min using a Grass stimulator (Grass Technologies, West Warwick, RI, USA). Once the heart rate and pressure were stabilized, the perfusate was

switched to modified KH buffer containing 30 μM $MnCl_2$ for 30 min (the wash-in period), followed by a 30-min wash-out period with Mn^{2+}-free buffer. During Mn^{2+} perfusion, phosphate and sulfate were replaced with chloride in the modified KH buffer to prevent Mn^{2+} precipitation. There were three experimental groups: 1, NCX inhibition by 1 μM SEA0400 during Mn^{2+} wash-in only (SEAin, $n = 6$); 2, NCX inhibition by 1 μM SEA0400 during Mn^{2+} wash-out only (SEAout, $n = 6$); 3, no NCX inhibition during both wash-in and wash-out to serve as the control group (CNTL, $n = 5$).

Image acquisition

The perfusion column was placed inside a 9.4-T vertical-bore spectrometer (Bruker Biospin Co., Billerica, MA, USA). Image acquisition used a 20-mm volume coil. A 1-mm-thick short-axis slice at the midventricular level was prescribed for imaging. A triggered saturation–recovery Look–Locker sequence was used for rapid T_1 mapping (18). Pacing signals were used to trigger the image acquisition. Prior to Mn^{2+} perfusion, two baseline T_1 maps were acquired. To delineate the kinetics of Mn^{2+}-induced contrast enhancement, sequential T_1 maps were acquired at a temporal resolution of 3 min during the Mn^{2+} wash-in and wash-out periods. Imaging parameters were as follows: TE, 2 ms; TR, trigger interval, 166 ms; flip angle, 10°; field of view, 2.5 × 2.5 cm^2; matrix size, 128 × 64. At the end of imaging acquisition, hearts were frozen in liquid nitrogen for the quantification of Mn^{2+} content by flame atomic absorption spectrophotometry. To quantify the Mn^{2+} content at the end of Mn^{2+} wash-in, an additional set of hearts was frozen at the end of the wash-in period.

Image analysis

Image analysis used in-house-developed MATLAB-based software described in detail previously (18). T_1 maps of the whole heart were generated by performing pixel-wise curve fitting. The myocardial free wall was selected as the region of interest to quantify the changes in the T_1 relaxation time during the imaging protocol.

Mn^{2+} quantification by flame atomic absorption spectrophotometry

Frozen ventricular tissues were burned in a furnace at 600 °C for 2 h. The ashes were dissolved in 20% nitric acid. The Mn^{2+} content was measured by a flame atomic absorption spectrophotometer (Buck Scientific, Norwalk, CT, USA).

Mn^{2+} toxicity on isolated myocytes

To evaluate the cardiotoxicity of Mn^{2+}, myocyte shortening and Ca^{2+} transients were measured in isolated mouse myocytes. Briefly, mice were anesthetized with pentobarbital (85 mg/kg) and heparin (1000 units/kg). The heart was excised, cannulated and perfused with Ca^{2+}-free Tyrode solution containing 0.8 mg/mL collagenase type II (Worthington Biochemical Co., Lakewood, NJ, USA) for 5 min. The original Tyrode solution contained (in mM): NaCl, 136; KCl, 5.4; $MgCl_2$, 1.0; HEPES, 10; NaH_2PO_4, 1.2; glucose, 5.6; L-glutamine, 2; taurine, 5. The heart was then removed from the perfusion column. The ventricles were minced, gently agitated and rinsed. Isolated myocytes were collected and incubated in Media 199 (GIBCO, Grand Island, NY, USA) containing 1.8 mM Ca^{2+} and 0, 50, 100 and 500 μM of $MnCl_2$, respectively, for 1 h. The temperature and pH were maintained at 37°C and pH 7.2–7.4, respectively.

Myocytes were placed in a glass-bottomed Petri dish on the stage of an Olympus IX71 inverted fluorescence microscope (Olympus America, Center Valley, PA, USA). Myocyte contractility was evaluated by calculating the maximum fractional shortening from changes in cell length during 1-Hz stimulation using a Grass stimulator (Grass Technologies). To measure Ca^{2+} transients, myocytes were incubated at 37 °C with 1 μM fura-2-

acetoxymethyl ester for 15 min, and the extra dye was washed out. The dye was excited at 340 and 380 nm using a xenon arc lamp through a computer-controlled high-speed random access monochromator (Photon Technology International, Birmingham, NJ, USA). The fluorescent signals were detected at 510 nm by an analog/photon counting photomultiplier detector (Photon Technology International). Ca^{2+} transients were calculated as the ratio of the detected fluorescence in response to 340 and 380-nm excitation wavelengths (F_{340}/F_{380}), respectively, using in-house-developed MATLAB software.

Statistical analysis

All the data are expressed as the mean ± standard deviation. Mean values in the CNTL, SEAin and SEAout groups were compared by one-way analysis of variance. If there were statistical differences, multiple pairwise comparisons were performed using Tukey's test. $P < 0.05$ was considered to be statistically significant.

RESULTS

Impact of Mn^{2+} on myocyte shortening and Ca^{2+} transients

At a concentration of 50 μM, Mn^{2+} had no obvious impact on myocyte contractility and Ca^{2+} handling (Fig. 1). Both myocyte shortening and Ca^{2+} transients were similar to those of the control myocytes [p = not significant]. At 100 μM Mn^{2+} concentration, peak Ca^{2+} transients remained normal. However, myocyte shortening was decreased significantly from 8.65 ± 1.15% without Mn^{2+} to 6.21 ± 1.43% ($p < 0.005$). At 500 μM Mn^{2+} concentration, both myocyte shortening and peak Ca^{2+} transients were significantly reduced ($p < 0.001$). In addition, the baseline fluorescence ratio increased significantly ($p < 0.001$).

Animal characteristics and contractile function

The age, body weight and heart weight of the animals are listed in Table 1. There were no significant differences among the three groups. Figure 2a shows the time course of RPP changes during the imaging protocol. Ventricular pressure and RPP before Mn^{2+} perfusion (baseline), as well as during Mn^{2+} wash-in and wash-out, are listed in Table 2. Mn^{2+} perfusion showed no impact on ventricular function. However, NCX inhibition with SEA0400 induced a significant increase in both LVSP and LVEDP, with LVSP increased to a greater extent ($p < 0.001$). As a result, both LVDP and RPP increased significantly in the SEAin and SEAout groups when compared with the controls ($p < 0.001$).

T_1 changes during wash-in and wash-out

Figure 3a shows representative T_1 maps at baseline, at the end of Mn^{2+} wash-in and at the end of the wash-out period. The time courses of R_1 changes during the imaging protocol are shown in Fig. 2b. All three groups showed a progressive increase in R_1 during the wash-in period. However, the SEAin group exhibited an accelerated increase in R_1. After 3 min of Mn^{2+} perfusion, R_1 in the SEAin group was significantly higher than that in the other two groups ($p < 0.05$). At the end of Mn^{2+} wash-in, the R_1 values were 1.61 ± 0.18, 1.88 ± 0.28 and 1.62 ± 0.21 s^{-1} for the CNTL, SEAin and SEAout groups, respectively (Fig. 3b).

All three groups showed a slight decrease in R_1 during the wash-out period (Fig. 2b). The R_1 decrease was smallest in the SEAout group. At the end of wash-out, R_1 in both the SEAout and SEAin groups was significantly higher than that in the CNTL group (Fig. 3b, $p < 0.05$). The R_1 values at the end of wash-out were 1.36 ± 0.17, 1.70 ± 0.32 and 1.65 ± 0.10 s^{-1} for CNTL, SEAin and SEAout groups, respectively.

The wash-out curves were fitted to two exponential functions, i.e. $y = A\ e^{-t/B}$ and $y = A\ e^{-t/B} + C$, respectively. The fitted parameters are listed in Table 3. Using a simple

exponential curve fitting ($y = A\ e^{-t/B}$), the mean half-times for R_1 reduction were 3.18, 4.25 and 6.66 h for the CNTL, SEAin and SEAout groups, respectively. Using an expoenntial function with a constant term ($y = A\ e^{-t/B} + C$), the fitted time constant was reduced significantly for all three groups. The C/A ratio ranged from 5.87 to 10.71.

Myocardial Mn^{2+} content

Consistent with MRI findings, NCX inhibition increased significantly the Mn^{2+} content in SEAin hearts (12.9 ± 1.6 μg/g wet weight) at the end of wash-in when compared with controls (8.2 ± 0.2 μg/g wet weight) (Fig. 3c, p <0.001). Perfusion with Mn^{2+}-free buffer caused a significant decrease in myocardial Mn^{2+} content at the end of wash-out in CNTL hearts (6.3 ± 0.9 μg/g wet weight, $p < 0.005$). NCX inhibition led to increased Mn^{2+} retention in the SEAout group (9.5 ± 3.0 μg/g wet weight) when compared with the CNTL group (Fig. 3c, $p < 0.05$). As a result of increased Mn^{2+} accumulation during the wash-in period, SEAin hearts also showed elevated Mn^{2+} content at the end of wash-out (9.1 ± 2.5 μg/g wet weight) when compared with the CNTL group (Fig. 3c, $p < 0.05$).

DISCUSSION

The major findings of the present study were that, in perfused rat hearts, the Mn^{2+} content and T_1 mapping with MEMRI were dependent on SEA0400 and thus, presumably, on NCX activity. Previously, Waghorn *et al.* (15,16) have investigated Mn^{2+} retention in an *in vivo* mouse study. They observed that treatment with SEA0400 reduced significantly the rate of decrease in ΔR_1 hours after Mn^{2+} infusion was withdrawn. In the current study, we used a fast T_1 mapping method to follow the dynamic changes in R_1 during Mn^{2+} perfusion and wash-out. Our results suggest that altered Mn^{2+} efflux via NCX is reflected in R_1 changes during both wash-in and wash-out.

Physiologically, Ca^{2+} entry into myocytes via L-type Ca^{2+} channels is balanced by its efflux through NCX (1). Although Mn^{2+} also enters the myocytes through L-type Ca^{2+} channels, its efflux via NCX has been considered to be negligible because of the long Mn^{2+} retention time. However, recent studies by Waghorn *et al.* (15,16) have shown that differences in R_1 changes induced by NCX inhibition can be observed 4 h after Mn^{2+} withdrawal. With NCX inhibition, these authors observed an increase in the half-time of ΔR_1 reduction from 3.4 h (without SEA0400) to 5.6 h (with SEA0400) in mouse hearts. In the current study, the estimated half-time for R_1 reduction increased from 3.18 h with-out SEA0400 to 6.66 h in the presence of SEA0400, which was similar to that reported by Waghorn *et al.* The average half-time for R_1 reduction in the SEAin group (4.25 h) was also higher than that in the controls because of the incomplete elimination of the inhibitor during the wash-out period (19). Consistent with the MRI findings, the Mn^{2+} content at the end of the wash-out period was also significantly higher in hearts perfused with SEA0400 than in the control group.

It is interesting to note that, when the wash-out curves were fitted to an exponential function with a constant term, the fitted time constant was significantly reduced by an order of magnitude (Table 3). Moreover, the ratio of the constant term to the exponential term (C/A) was more than five-fold in all three groups, which may suggest the existence of a large Mn^{2+} pool that is washed away very slowly.

With NCX inhibition by SEA0400, the R_1 values at the end of the wash-in period increased in the SEAin group when compared with hearts without the inhibitor (SEAout and CNTL groups), suggesting increased Mn^{2+} accumulation in the presence of the NCX inhibitor during the wash-in period. Atomic absorption spectroscopy analysis of hearts at the end of the wash-in period also showed that the Mn^{2+} content in the SEAin group increased by 57% compared with the other two groups. As SEA0400 does not enhance Ca^{2+} channel activity

under normal physiological conditions (20), this increased Mn^{2+} accumulation presumably reflects reduced Mn^{2+} efflux via NCX. These data suggest that MEMRI with fast T_1 mapping may provide a tool for the evaluation of NCX activity.

The contribution of NCX to Ca^{2+} extrusion from myocytes is species dependent (21,22). Sham *et al.* (21) evaluated the rates of Ca^{2+} removal in isolated myocytes from rat, guinea-pig, hamster ventricles and human atria. Their study suggests that NCX activity in the rat ventricle is lower than that in hamsters, guinea-pigs and humans. As such, larger animals and humans may manifest a greater Mn^{2+} efflux rate than that observed in rats in the current study. However, careful further investigations are necessary to evaluate whether this difference in NCX contribution to Ca^{2+} extrusion will render MEMRI more sensitive to alterations in NCX activity in large animals and humans.

The inhibition of NCX also induced a small increase in LVDP. This result is consistent with previous studies on perfused rat hearts (23,24). Previously, Acsai *et al.* (20) have reported an increase in myocyte shortening in isolated rat myocytes incubated with SEA0400. In addition, they observed an increase in Ca^{2+} transients and a trend of increase in diastolic Ca^{2+} level. However, this increase in cytosolic Ca^{2+} was not accompanied by an increase in the L-type Ca^{2+} current. Therefore, the observed increase in Ca^{2+} transients is probably caused by the blockage of Ca^{2+} efflux via NCX, leading to increased ventricular contractility.

Because both Mn^{2+} uptake and efflux can have an impact on the dynamics of R_1 during Mn^{2+} infusion, care must be taken in interpreting the data. In general, the determination of both influx and efflux rates from a single wash-in curve is underdetermined unless other constraints are imposed in parameter estimation. In the current experimental settings, the measured R_1 dynamics during wash-out can provide additional data to constrain curve fitting. For *in vivo* studies, the measurement of the Mn^{2+} content in blood, i.e. the arterial input function, can also provide additional constraints for curve fitting. However, such an approach requires fast and accurate T_1 mapping in both myocardium and blood.

In summary, we have investigated the sensitivity of MEMRI to NCX inhibition via SEA0400. Our results show that, in rat hearts, MEMRI with fast T_1 mapping is sensitive to SEA0400-dependent changes in Mn^{2+} accumulation and retention. Although these results suggest that MEMRI has the potential to detect altered NCX activity, further investigation is needed to assess the sensitivity of MEMRI to more subtle changes in NCX activity under disease conditions.

Acknowledgments

This work was supported by grants from the National Heart, Lung and Blood Institute (R01 HL-73315 and HL-86935 X. Yu).

Abbreviations used

EC	excitation–contraction
HR	heart rate
KH	Krebs–Henseleit
LVDP	left ventricular developed pressure
LVEDP	left ventricular end-diastolic pressure
LVSP	left ventricular systolic pressure

MEMRI	manganese-enhanced MRI
NCX	Na^+–Ca^{2+} exchanger
RPP	rate–pressure product
SR	sarcoplasmic reticulum

References

1. Bers DM. Cardiac excitation–contraction coupling. Nature. 2002; 415:198–205. [PubMed: 11805843]
2. Bassani JW, Bassani RA, Bers DM. Relaxation in rabbit and rat cardiac cells: species-dependent differences in cellular mechanisms. J Physiol. 1994; 476:279–293. [PubMed: 8046643]
3. Bassani RA, Bers DM. Na–Ca exchange is required for rest-decay but not for rest-potentiation of twitches in rabbit and rat ventricular myocytes. J Mol Cell Cardiol. 1994; 26:1335–1347. [PubMed: 7869394]
4. Pogwizd SM, Schlotthauer K, Li L, Yuan W, Bers DM. Arrhythmogenesis and contractile dysfunction in heart failure: roles of sodium–calcium exchange, inward rectifier potassium current, and residual beta-adrenergic responsiveness. Circ Res. 2001; 88:1159–1167. [PubMed: 11397782]
5. Guatimosim S, Guatimosim C, Song LS. Imaging calcium sparks in cardiac myocytes. Methods Mol Biol. 2011; 689:205–214. [PubMed: 21153794]
6. Nichols CB, Rossow CF, Navedo MF, Westenbroek RE, Catterall WA, Santana LF, McKnight GS. Sympathetic stimulation of adult cardiomyocytes requires association of AKAP5 with a subpopulation of L-type calcium channels. Circ Res. 2010; 107:747–756. [PubMed: 20671242]
7. Choi BR, Salama G. Simultaneous maps of optical action potentials and calcium transients in guinea-pig hearts: mechanisms underlying concordant alternans. J Physiol. 2000; 529(Pt 1):171–188. [PubMed: 11080260]
8. Wendland MF. Applications of manganese-enhanced magnetic resonance imaging (MEMRI) to imaging of the heart. NMR Biomed. 2004; 17:581–594. [PubMed: 15761947]
9. Mendonca-Dias MH, Gaggelli E, Lauterbur PC. Paramagnetic contrast agents in nuclear magnetic resonance medical imaging. Semin Nucl Med. 1983; 13:364–376. [PubMed: 6359418]
10. Hunter DR, Haworth RA, Berkoff HA. Cellular manganese uptake by the isolated perfused rat heart: a probe for the sarcolemma calcium channel. J Mol Cell Cardiol. 1981; 13:823–832. [PubMed: 6271977]
11. Brurok H, Schjott J, Berg K, Karlsson JO, Jynge P. Manganese and the heart: acute cardiodepression and myocardial accumulation of manganese. Acta Physiol Scand. 1997; 159:33–40. [PubMed: 9124068]
12. Medina DC, Kirkland DM, Tavazoie MF, Springer CS Jr, Anderson SE. Na^+/Ca^{2+}-exchanger-mediated Mn^{2+}-enhanced ^1H_2O MRI in hypoxic, perfused rat myocardium. Contrast Media Mol Imaging. 2007; 2:248–257. [PubMed: 18050358]
13. Hu TC, Pautler RG, MacGowan GA, Koretsky AP. Manganese-enhanced MRI of mouse heart during changes in inotropy. Magn Reson Med. 2001; 46:884–890. [PubMed: 11675639]
14. Krombach GA, Saeed M, Higgins CB, Novikov V, Wendland MF. Contrast-enhanced MR delineation of stunned myocardium with administration of $MnCl_2$ in rats. Radiology. 2004; 230:183–190. [PubMed: 14695393]
15. Waghorn B, Yang Y, Baba A, Matsuda T, Schumacher A, Yanasak N, Hu TC. Assessing manganese efflux using SEA0400 and cardiac T_1-mapping manganese-enhanced MRI in a murine model. NMR Biomed. 2009; 22:874–881. [PubMed: 19593760]
16. Waghorn B, Schumacher A, Liu J, Jacobs S, Baba A, Matsuda T, Yanasak N, Hu TC. Indirectly probing Ca^{2+} handling alterations following myocardial infarction in a murine model using T_1-mapping manganese-enhanced magnetic resonance imaging. Magn. Reson. Med. 2011; 65:239–249.

17. Matsuda T, Arakawa N, Takuma K, Kishida Y, Kawasaki Y, Sakaue M, Takahashi K, Takahashi T, Suzuki T, Ota T, Hamano-Takahashi A, Onishi M, Tanaka Y, Kameo K, Baba A. SEA0400, a novel and selective inhibitor of the Na^+–Ca^{2+} exchanger, attenuates reperfusion injury in the in vitro and in vivo cerebral ischemic models. J. Pharmacol. Exp. Ther. 2001; 298:249–256.
18. Li W, Griswold M, Yu X. Rapid T_1 mapping of mouse myocardium with saturation recovery Look–Locker method. Magn. Reson. Med. 2010; 64:1296–1303.
19. Iwamoto T, Kita S, Uehara A, Imanaga I, Matsuda T, Baba A, Katsuragi T. Molecular determinants of Na^+/Ca^{2+} exchange (NCX1) inhibition by SEA0400. J. Biol. Chem. 2004; 279:7544–7553.
20. Acsai K, Kun A, Farkas AS, Fulop F, Nagy N, Balazs M, Szentandrassy N, Nanasi PP, Papp JG, Varro A, Toth A. Effect of partial blockade of the Na^+/Ca^{2+}-exchanger on Ca^{2+} handling in isolated rat ventricular myocytes. Eur J Pharmacol. 2007; 576:1–6. [PubMed: 17727839]
21. Sham JS, Hatem SN, Morad M. Species differences in the activity of the Na^+–Ca^{2+} exchanger in mammalian cardiac myocytes. J Physiol. 1995; 488(Pt 3):623–631. [PubMed: 8576853]
22. Tanaka H, Namekata I, Nouchi H, Shigenobu K, Kawanishi T, Takahara A. New aspects for the treatment of cardiac diseases based on the diversity of functional controls on cardiac muscles: diversity in the excitation–contraction mechanisms of the heart. J Pharmacol Sci. 2009; 109:327–333. [PubMed: 19270426]
23. Farkas AS, Acsai K, Nagy N, Toth A, Fulop F, Seprenyi G, Birinyi P, Nanasi PP, Forster T, Csanady M, Papp JG, Varro A, Farkas A. Na^+/Ca^{2+} exchanger inhibition exerts a positive inotropic effect in the rat heart, but fails to influence the contractility of the rabbit heart. Br J Pharmacol. 2008; 154:93–104. [PubMed: 18332852]
24. Szentandrassy N, Birinyi P, Szigeti G, Farkas A, Magyar J, Toth A, Csernoch L, Varro A, Nanasi PP. SEA0400 fails to alter the magnitude of intracellular Ca^{2+} transients and contractions in Langendorff-perfused guinea pig heart. Naunyn Schmiedebergs Arch. Pharmacol. 2008; 378:65–71.

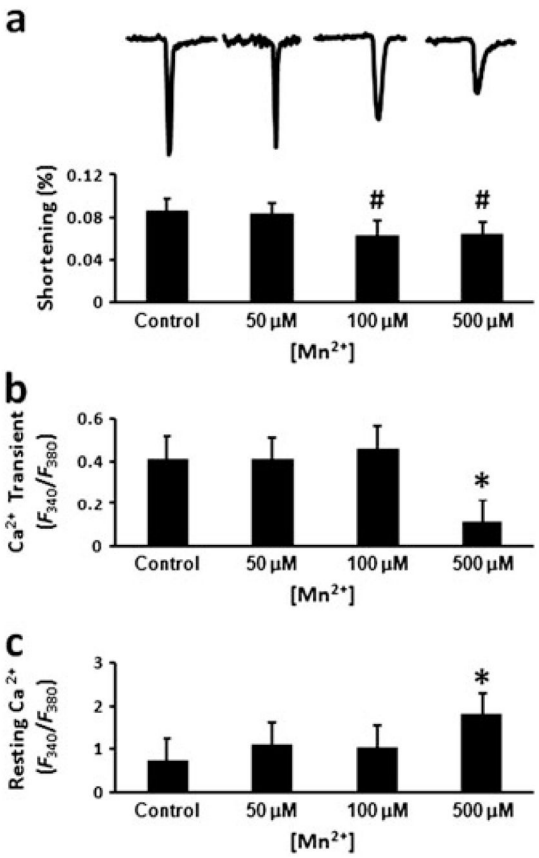

Figure 1.

Manganese (Mn^{2+}) toxicity on isolated myocytes. (a) Representative recordings of changes in myocyte length during electrical stimulation and the calculated fractional shortening. (b) Peak calcium (Ca^{2+}) transients. (c) Resting intracellular Ca^{2+} concentration. #$p < 0.005$ compared with the control; *$p < 0.0001$ compared with the other groups.

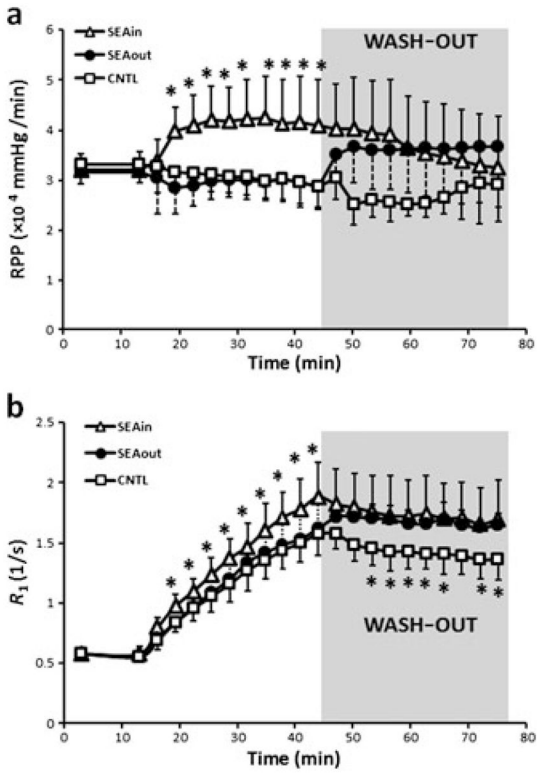

Figure 2.

Time courses of rate–pressure product (RPP) (a) and relaxation rate (R_1) (b) during imaging protocol. Shaded areas indicate the wash-out period. Sodium–calcium (Na^+–Ca^{2+}) exchanger (NCX) inhibition was induced by 1 μM SEA0400 during either manganese (Mn^{2+}) perfusion (SEAin) or wash-out (SEAout). *$p < 0.05$ compared with control (CNTL).

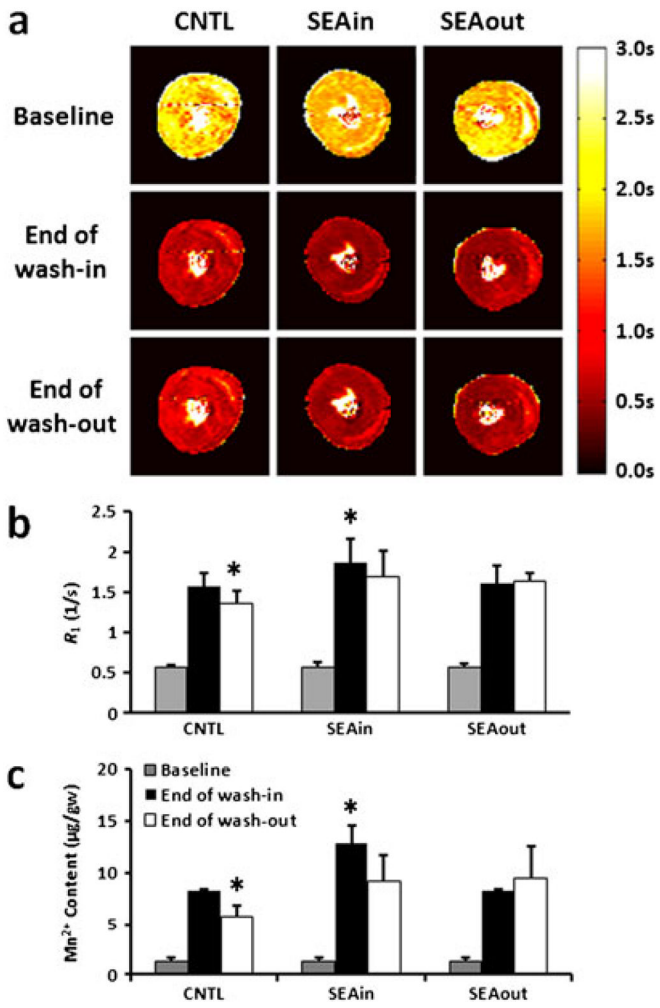

Figure 3.

Longitudinal relaxation time (T_1), rate (R_1) and manganese (Mn^{2+}) content. (a) Representative T_1 maps before Mn^{2+} perfusion (baseline), at the end of Mn^{2+} wash-in and at the end of wash-out. Relaxation rate (R_1) (b) and Mn^{2+} content (c) at the corresponding time points. Sodium–calcium (Na^+–Ca^{2+}) exchanger (NCX) inhibition was induced by 1 μM SEA0400 during either Mn^{2+} perfusion (SEAin) or wash-out (SEAout). *$p < 0.05$ compared with the other two groups at the same time points. CNTL, control.

Table 1

Animal characteristics

	Age (weeks)	Body weight (g)	Heart weight (g)
Control (n = 5)	8.89 ± 0.91	317.20 ± 22.13	1.54 ± 0.12
SEA0400 wash-in (n = 6)	9.40 ± 0.76	334.01 ± 16.87	1.58 ± 0.27
SEA0400 wash-out (n = 6)	9.86 ± 0.62	332.33 ± 26.55	1.66 ± 0.27

Table 2

Ventricular function during the imaging protocol

		Baseline	Wash-in	Wash-out
Control (n = 5)	LVSP (mmHg)	90.58 ± 5.85	84.16 ± 10.81	74.95 ± 8.30[b]
	LVEDP (mmHg)	1.25 ± 1.68	3.04 ± 1.83	3.45 ± 1.30
	LVDP (mmHg)	88.40 ± 6.97	81.96 ± 10.61	71.40 ± 8.70[b]
	RPP ($\times 10^4$ mmHg/min)	3.32 ± 0.20	3.06 ± 0.39	2.60 ± 0.32[b]
SEA0400 wash-in (n = 6)	LVSP (mmHg)	90.94 ± 8.25	113.20 ± 19.10[a]	102.09 ± 26.45[a]
	LVEDP (mmHg)	2.92 ± 0.79	1.73 ± 1.44[a]	1.50 ± 1.61[a]
	LVDP (mmHg)	87.97 ± 9.02	111.47 ± 19.72[a]	100.59 ± 26.84[a]
	RPP ($\times 10^4$ mmHg/min)	3.21 ± 0.33	4.07 ± 0.72[a]	3.67 ± 0.98[a]
SEA0400 wash-out (n = 6)	LVSP (mmHg)	88.68 ± 5.25	84.94 ± 10.83	101.51 ± 22.07[a]
	LVEDP (mmHg)	1.19 ± 2.07	2.78 ± 1.71	1.18 ± 2.38[a]
	LVDP (mmHg)	86.58 ± 5.75	81.12 ± 11.62	99.31 ± 23.39[a]
	RPP ($\times 10^4$ mmHg/min)	3.16 ± 0.21	2.96 ± 0.42	3.61 ± 0.86[a]

LVDP, left ventricular developed pressure; LVEDP, left ventricular end-diastolic pressure; LVSP, left ventricular systolic pressure; RPP, rate–pressure product.

[a] $p < 0.001$ compared with the control group at the same time point.

[b] $p < 0.05$ compared with baseline in the same group.

Table 3

Time constants of R_1 decrease during the wash-out period

$y = A\ e^{-t/B}$				$y = A\ e^{-t/B} + C$			
	Control	**SEA0400 wash-in**	**SEA0400 wash-out**		**Control**	**SEA0400 wash-in**	**SEA0400 wash-out**
A	1.63	1.80	1.72	A	0.24	0.16	0.23
B (h)	4.57	6.09	9.62	B (h)	0.42	0.22	1.07
				C	1.40	1.67	1.49
				C/A	5.87	10.71	6.44
R^2	0.94	0.82	0.74	R^2	0.96	0.88	0.74